JACS
JOURNAL OF THE AMERICAN CHEMICAL SOCIETY
pubs.acs.org/JACS
Article

Extended Hydrogen Bond Networks for Effective Proton-Coupled Electron Transfer (PCET) Reactions: The Unexpected Role of Thiophenol and Its Acidic Channel in Photocatalytic Hydroamidations

Nele Berg, Sebastian Bergwinkl, Patrick Nuernberger, Dominik Horinek, and Ruth M. Gschwind*

Cite This: J. Am. Chem. Soc. 2021, 143, 724−735
Read Online
ACCESS | Metrics & More | Article Recommendations | Supporting Information

ABSTRACT: Preorganization and aggregation in photoredox catalysis can significantly affect reactivities or selectivities but are often neglected in synthetic and mechanistic studies, since the averaging effect of flexible ensembles can effectively hide the key activation signatures. In addition, aggregation effects are often overlooked due to highly diluted samples used in many UV studies. One prominent example is Knowles's acceleration effect of thiophenol in proton-coupled electron transfer mediated hydroamidations, for which mainly radical properties were discussed. Here, cooperative reactivity enhancements of thiophenol/disulfide mixtures reveal the importance of H-bond networks. For the first time an in-depth NMR spectroscopic aggregation and H-bond analysis of donor and acceptor combined with MD simulations was performed revealing that thiophenol acts also as an acid. The formed phosphate-H^+-phosphate dimers provide an extended H-bond network with amides allowing a productive regeneration of the photocatalyst to become effective. The radical and acidic properties of PhSH were substituted by Ph_2S_2 and phosphoric acid. This provides a handle for optimization of radical and ionic channels and yields accelerations up to 1 order of magnitude under synthetic conditions. Reaction profiles with different light intensities unveil photogenerated amidyl radical reservoirs lasting over minutes, substantiating the positive effect of the H-bond network prior to radical cyclization. We expect the presented concepts of effective activation via H-bond networks and the reactivity improvement via the separation of ionic and radical channels to be generally applicable in photoredox catalysis. In addition, this study shows that control of aggregates and ensembles will be a key to future photocatalysis.

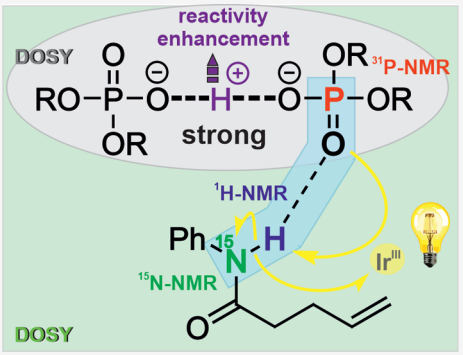

INTRODUCTION

Light dependent as well as light independent proton-coupled electron transfer (PCET) reactions play an essential role in biological systems,[1−13] e.g. for the O_2 generation in the photosystem II.[14] Their potential was also successfully applied in electrochemistry,[2,15−24] transition metal chemistry,[1,25,28] and photochemical transformations.[1,2,29−45] In synthetic organic chemistry the activation of strong covalent bonds, such as C−H, O−H, and N−H, is a very challenging task to access important synthetic building blocks. To overcome their high energy barriers in an atom economic and environmentally friendly manner, the combination of PCET and photocatalysis paved the way to an efficient reaction design. Especially, the photocatalytic concerted multisite PCET (MS-PCET) was found to be successful.[2,36,46] There, a decoupled proton and electron transfer event in one elementary step omits highly energetic intermediates, which usually arise in conventional hydrogen atom transfer (HAT). In the oxidative MS-PCET, a proton and an electron originating from the same donor bond are transferred to a base and to a separate oxidant.[1,2,18] As a result, the proton and electron affinities of the two acceptor compounds can be fine-tuned independently allowing the activation of strong bonds which are not easily accessible via conventional redox processes.[36−38,47]

Thus, in the field of photocatalytic organic chemistry, using PCET, the group of Knowles transformed ketones into cyclic alcohols,[34,42,48] activated N−H bonds in extensive hydro-/carboamination and hydro-/carboamidation protocols, opened cyclic alcohols via PCET mediated alkoxy radical generation,[31,32,35,41,43,44,49] and succeeded even in the alkylation of remote C−H bonds via an amide PCET process.[33] More recently, they developed an aliphatic C−H bond activation[50] and a PCET driven NH_3 synthesis.[51] Even for the deracemization of ureas, PCET is involved.[52] Further coupling reactions were recently designed including an aldehyde−olefin

Received: August 12, 2020
Published: January 11, 2021

https://dx.doi.org/10.1021/jacs.0c08673
J. Am. Chem. Soc. 2021, 143, 724−735

coupling via reductive ketyl radical formation,[29] the generation of pyridine based heterocycles,[53] and the copper-based photocatalytic coupling of ketones.[54] Moreover, the PCET concept was employed in visible light mediated selective C−C bond cleavage of lignines[55] and the C−H functionalization of cyclic ethers.[56]

In such light driven oxidative PCET reactions the formation of a D−H···A hydrogen bond (H-bond) between the D−H bond to be cleaved and the applied base A (Figure 1a) is stated

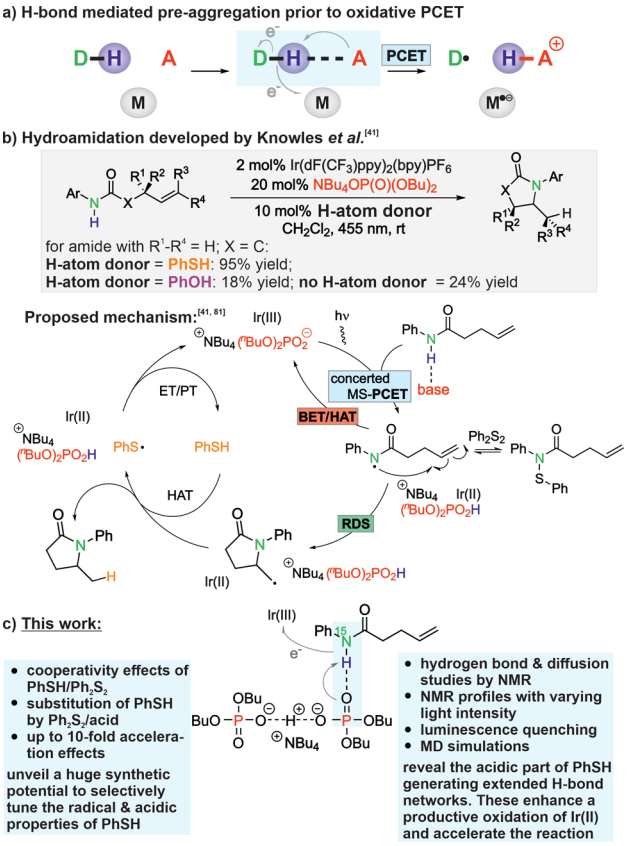

Figure 1. (a) An H-bonded preaggregate is proposed as the key interaction for a selective cleavage of strong bonds via PCET in literature. (b) The photocatalytic hydroamidation of phenylamides developed by Knowles was chosen as the model system. Its postulated light driven mechanism involves an excited state iridium catalyst and a phosphate base for the crucial PCET step, thiophenol as the HAT donor and a highly effective unproductive BET. The N−H cleavage in the presence of weaker S−H bonds is surprising concerning the BDFEs (see main text). (c) Our studies reveal the potential to selectively access the radical and ionic properties of PhSH by the formation of extended H-bonded aggregates allowing for a productive back oxidation of Ir(II) prior to radical cyclization.

to be responsible for lowering the reaction energy barrier.[1,2,37,36,47,51−58] Especially, the proton transfer requires an overlap of the vibronic states and thus a minimized donor−acceptor distance. Hence, the formation of strong donor−acceptor H-bonded preaggregates is proposed for the initiation of PCET.[1,2,46] Furthermore, the geometry and strength of the H-bond seem to be essential as shown for competing mechanisms, HAT versus PCET in benzyl/toluene pairs and phenoxy/phenol aggregates.[59,60] Internal H-bonds of the latter aggregate were shown to accelerate the coupled electron proton transfer rate in a pH independent manner.[61] The formation of a H-bond was even found to suppress a HAT mechanism due to steric reasons.[62] As expected, charge assisted H-bonds and solvents promoting strong H-bonds accelerate charge transfer events for an efficient PCET process.[63,64] Moreover, using IR spectroscopy, H-bond equilibrium constants were determined for a TEMPOH/pyridine complex.[65]

Computational studies on model systems in biology, biochemistry, solution chemistry, and electrochemistry corroborated the essential role of H-bond formation for PCET, e.g. enhancing the vibronic donor−acceptor coupling.[3,12,17,18,66,67] For example, the PCET driven aerobic respiratory chain[3,17] and effects of antioxidants[68−70] were shown to occur via the formation of H-bond mediated aggregates.

In contrast, experimental studies are scarce in the field of photocatalytic PCET reactions. Via EPR spectroscopy, a strong H- bonded complex between histidine and a benzoquinone derivative (TolSQ) was detected.[71] Furthermore, combined NMR, transient absorption, and emission spectroscopic investigations demonstrated a correlation between H-bond strengths and charge transfer kinetics in model systems, using exclusively ^{1}H chemical shift changes for the H-bond analysis.[63,64] Later, by applying a combination of ^{1}H NMR spectroscopy and cyclic voltammetry, this trend was further corroborated for an electrochemical reaction.[72] Via ^{1}H NMR titration experiments a phenol−pyridine interaction was identified.[73] Knowles and Alexanian even examined a non-covalent interaction between the iridium photocatalyst and a phosphate base to be responsible for successful C−H bond activation.[50]

One prominent example deviating from the general mechanistic concept of concerted MS-PCET is the accelerating effect of thiophenol in the oxidative photocatalytic hydroamidation of phenylamides developed by Knowles and co-workers (Figure 1b).[32] In the proposed mechanism, the excited state of the photocatalyst acts as electron acceptor and a phosphate base as the proton acceptor for the activation of the amide substrate in a H-bonded amide/base preaggregate, followed by the intramolecular addition of the formed amidyl radical to the olefin. In a final HAT step involving thiophenol (PhSH) as the hydrogen atom donor, the lactam product is furnished in up to 95% yield; however phenol (PhOH), which is a commonly known HAT transfer reagent, was unproductive.[32] PhSH as the HAT donor was applied in other synthetic protocols,[74−76] and other groups showed that the S−H bond can be directly activated via PCET reactions.[77−79] The chemoselectivity factors for the selective cleavage of the stronger amide N−H group was recently explained by Knowles via a combination of H-bond networks and PCET kinetics.[80] However, the luminescence quenching experiments in these studies were conducted at highly diluted concentrations not addressing the complex aggregation and H-bond networks expected for ion pairs and amides in apolar organic solvents.[32,80] An in-depth kinetic study of Nocera revealed the importance of the overall performance of the PCET/back-electron transfer (BET) equilibria for quantum efficiency in these hydroamidations.[81] By adding disulfides they allowed for an off-cycle equilibrium, could reduce the BET rate, and increased the concentration of the key amidyl radical available for the downstream reaction. However, both studies neglect the complex H-bond situation present at synthetic conditions and its potential to influence the PCET, BET, and corresponding back-proton transfer (BPT). Here, the central

https://dx.doi.org/10.1021/jacs.0c08673
J. Am. Chem. Soc. 2021, 143, 724−735

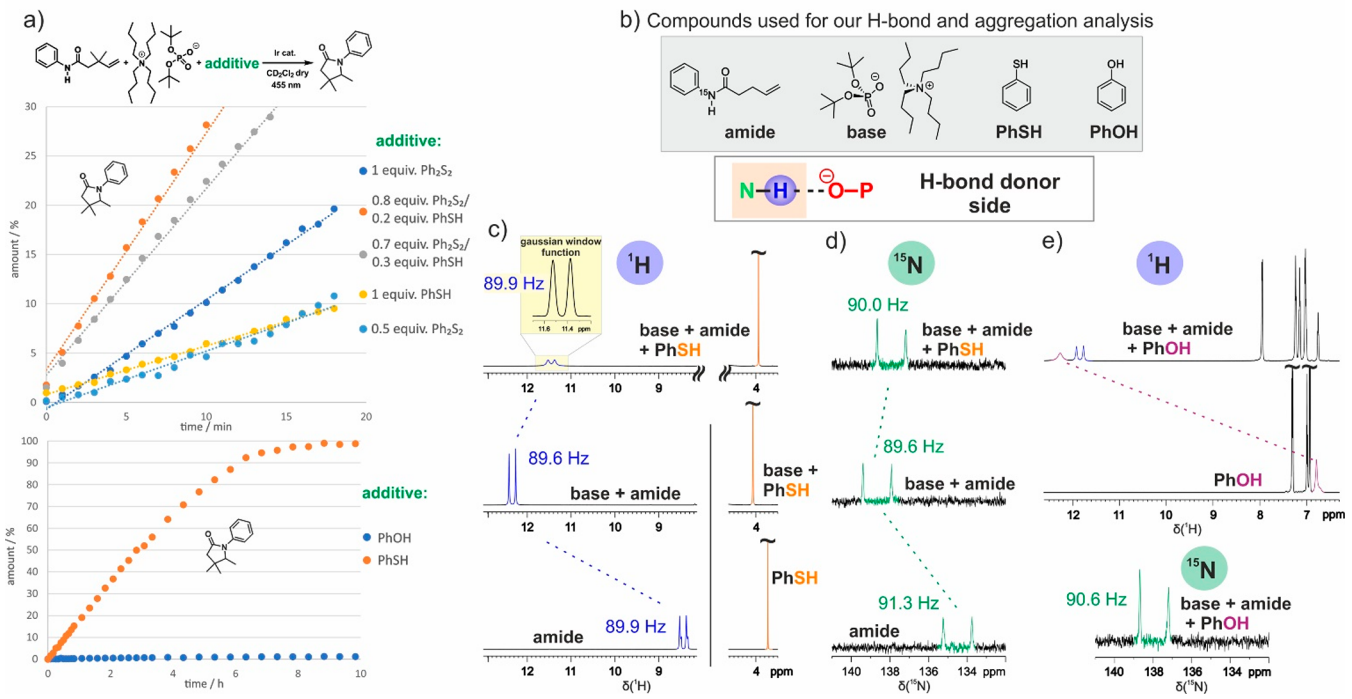

Figure 2. (a) The *in situ* NMR kinetics revealed a drastic acceleration of the overall PCET efficiency for mixtures of PhSh/Ph_2S_2 hinting at a H-bond effect in terms of cooperativity (top). The fast product formation (~100% after ~10 h) for the PhSH containing photocatalytic system and very low yields using PhOH (~1.2% after ~10 h) were confirmed by *in situ* NMR kinetics, too (bottom). The trend of the H-bond donor chemical shifts deviates from the PCET reactivities: (b) For the NMR spectroscopic H-bond investigations, ^{15}N-phenylpent-4-enamide (**amide**), tetrabutylammonium di*tert*-butylphosphate (**base**), thiophenol (**PhSH**) and phenol (**PhOH**) were used. The H-bond donor side was studied via (c) ^{1}H and (d) ^{15}N NMR chemical shift and scalar coupling analysis in CD_2Cl_2 at 180 K and 1:1/1:1:1 mixtures were used for the multicomponent samples. For the complete spectra, see SI. The amidyl $^{15}N-H$ low field shift in both 1D spectra in the presence of base confirmed the existence of an H-bond, which is weakened after adding PhSH. In contrast, PhSH is mainly free in solution as the δ-values are only barely affected. (e) A significant ^{1}H low field shift of the phenol OH proton indicates its incorporation into the H-bonded complex, but the amide chemical shifts are similar to the PhSH containing samples.

question is the role and effect of thiophenol on this H-bond network and the overall reaction rate.

Therefore, in this study first initial rate kinetics of mixtures of PhSH and diphenyldisulfide (Ph_2S_2) were investigated. These showed cooperativity effects beyond the additivity expected for the mere radical effect and underpinned the importance of the H-bond network. Next, for the first time an in-depth NMR spectroscopic analysis of the donor and acceptor side of the H-bonds of this PCET driven hydroamidation reaction was performed using low temperature ^{1}H, ^{15}N, ^{31}P chemical shifts and $^{1}J_{NH}$ scalar couplings (Figure 1c). These and diffusion measurements reveal an unexpected modulation of the H-bonded aggregates by thiophenol. Furthermore, these special aggregates were corroborated by MD-simulations, which is to the best of our knowledge the first time such a combined NMR/MD approach in chemical photoredox catalysis has been undertaken. Last but not least, PhSH was replaced by a combination of Ph_2S_2 and phosphoric acid, which allowed the ionic and the radical properties to be dissected and optimized separately. Luminescence quenching studies and reaction profiles with different light intensities were employed to dissect the various mechanistic steps and to reveal a productive regeneration pathway of Ir(II) to Ir(III) being affected by the extended H-bond network.

RESULTS AND DISCUSSION

Model System. The employed PCET model system in this work is directly derived from the synthetic conditions of the hydroamidation protocol of Knowles and co-workers.[32] For the *in situ* reaction kinetics 3,3-dimethyl-*N*-phenylpent-4-enamide was synthesized in order to exclude self-HAT. To get access to the H-bond donor side, a ^{15}N labeled *N*-phenylpent-4-enamide was synthesized. As a proton acceptor species, tetrabutylammonium di-*tert*-butylphosphate was used which showed excellent reactivity inside the photocatalytic reaction at room temperature (see SI chapter 3.1−3.4) and enables simplification of the spectra due to a reduced amount of NMR signals compared to the originally used *n*-butyl phosphate base. For the H-bond and aggregation studies, 1:1 mixtures (50 mM) of amide and phosphate as well as 1:1:1 mixtures of amide, phosphate, and thiol or phenol were prepared in dichloromethane-d_2 (CD_2Cl_2) and measured at 300 and 180 K.[82] Due to chemical exchange reduction at low temperature, specific H-bonded aggregates are visible on the NMR time scale.

Furthermore, dichloromethane was applied by the group of Knowles and is also suitable for our low temperature NMR studies.[31,32,83]

Initial Rate Kinetics Reveal Importance of H-Bonds. For phenol and thiophenols as additives, huge reactivity differences[32] were observed previously, which can be attributed to their pronounced distinctions in radical and HAT properties, potential catalyst inhibition, side reactions of phenol, or unproductive PCET activation of phenol. Our initial rate kinetics shown in Figure 2a (bottom) confirmed this reactivity difference. For phenol, no catalyst inhibition by the

https://dx.doi.org/10.1021/jacs.0c08673
J. Am. Chem. Soc. 2021, 143, 724−735

product and only marginal byproduct formation were found but significantly different H-bond networks were found. Thus, both different radical properties and different H-bond networks may contribute to dissimilar reactivities of phenol and thiophenol. The radical/HAT properties of thiophenol and phenol are so different that it is difficult to dissect the contributions of radical properties and the H-bond network between these two. Therefore, we investigated Ph_2S_2, PhSH, and mixtures of both. In agreement with Nocera's results, the system with 1 equiv of disulfide shows a faster reaction rate than that with 1 equiv of PhSH corroborating the importance of the off-cycle radical equilibrium for a reduced BET (Figure 2a; top). Most astonishing however are the data of the mixtures of Ph_2S_2 and PhSH (80:20 and 70:30). When considering mere radical effects, reaction rates between those of pure Ph_2S_2 and PhSH are expected in terms of additivity. However, compared to pure Ph_2S_2, significantly higher reaction rates, i.e. nonlinear effects, were detected. This indicates that aggregation may play a pivotal role in this reaction type, which is typical for complex H-bond networks and beyond mere radical properties of isolated molecules. We interpreted this special acceleration as a hint that H-bonds may really be important and may affect the PCET, the BPT back reaction, or other parts of the mechanistic cycle. The principal importance of the H-bond binding constants for this reaction was already outlined by Qiu and Knowles in terms of chemoselectivity.[80] However, in their study highly diluted samples were used, which study the interactions between single molecules but not within the complex aggregates existing under synthetic conditions (see DOSY studies below).

H-Bond Analysis by NMR. Therefore, in-depth H-bond studies were conducted next. In general, the formation of a H-bond influences the electronic environment of both, the H-bond donor and acceptor sites. The shift of the proton toward the acceptor leads to a change in electron density distribution by deshielding of donor and proton and shielding of the acceptor.[84−86] Thus, the strength of this noncovalent bond can be read out via NMR chemical shifts and scalar couplings.[83] Limbach and co-workers established a method for the determination of the H-bond strengths in a biological system using low temperature ^{1}H and ^{15}N chemical shift correlations.[83] This concept was already successfully applied in our group for the analysis of H-bonds in Brønsted acid catalysis.[87,88] Moreover, we recently investigated the importance of H-bond mediated interactions for the selective activation of strong single C−F bonds.[89]

H-Bond Donor and Reactivity Profile. First, the H-bond donor side was analyzed via ^{1}H and ^{15}N NMR chemical shifts and scalar coupling studies. An overview of the analyzed compounds is depicted in Figure 2b. The formation of a H-bond between amide and phosphate base is expected to go hand in hand with a low field shift for both the amidyl proton and nitrogen as well as a reduced ^{15}N−H scalar coupling. In Figure 2c and 2d, the details of the ^{1}H and ^{15}N NMR spectra of pure ^{15}N-phenylpent-4-enamide (bottom), the ^{15}N-amide/base (middle), and the ^{15}N-amide/base/thiophenol (top) mixtures are shown. For the applied concentration of 50 mM, the pure amide itself exists as an oligomer (for detailed studies, see SI chapter 4.6.4) and the signals of the ^{15}N−H functionality at 8.45/134.49 ppm (89.9/91.3 Hz) refer therefore to the amide−amide H-bond (Figure 2c,d). In the presence of phosphate base, both amide proton and nitrogen are drastically low field shifted and the coupling is reduced (12.34/138.65 ppm, 89.6/89.6 Hz) indicating a by far stronger H-bond of the amide to the phosphate in accordance to their H-bond donor and acceptor abilities (see SI chapter 4.4).[90] The addition of PhSH slightly weakens the ^{15}N−H···O−P H-bond, which was identified by the reduction of the chemical shifts and a small increase of the coupling constant (11.45/137.91 ppm, 89.9[91]/90.0 Hz). In contrast to the amide signals, the ^{1}H chemical shift changes of the thiol S−H proton with and without base and amide are quite small (3.73−4.07 ppm; see Figure 2c, orange signal) and, hence, denote minimal interaction with the phosphate base or the amide. Via ^{1}H,^{1}H NOESY experiments, we further confirmed that the average amide−phosphate interaction is slightly reduced upon addition of thiophenol (see SI chapter 4.6.3).

Next, the situation with PhOH as the HAT donor was investigated, which showed a drastically reduced reactivity compared to PhSH as the additive (see Figure 2a, bottom). The phenolic O−H proton signal, which is located at 6.79 ppm for pure phenol, is significantly shifted to higher ppm values (12.26 ppm) in the presence of amide and base indicating that phenol is incorporated in a complex network of considerably strong H-bonds (Figure 2e). Simultaneously, the amidyl ^{15}N−H doublet shows in principle similar chemical shift and scalar coupling values (11.84/137.95 ppm, 89.7/90.6 Hz) compared to the amide/base/PhSH sample in both ^{1}H and ^{15}N spectra even with a trend toward slightly stronger amide−phosphate H-bonds. As a result, the classical H-bond strength analysis using exclusively ^{1}H chemical shifts as the sensor suggests a similar H-bond activation of the amide in the presence of PhSH and PhOH and fails to explain the huge reactivity difference of these two HAT donors (see Figure 2a), which previously was mainly attributed to their different radical and HAT properties, potential catalyst inhibition, or side reactions of phenol.[80] The only detectable difference is the inclusion of phenol into the H-bond network in contrast to mainly free thiophenol. However, this simplified donor-only observation of H-bonds can also hide the full situation.

H-Bond Acceptor and Phosphate Dimer Formation. Therefore, next the H-bond acceptor side of these mixtures was analyzed by ^{31}P NMR measurements. According to the trend demonstrated via ^{1}H and ^{15}N NMR, the movement of the proton toward the base predicts a shielding of the acceptor and therefore a high field shift of the ^{31}P signal of the base. Furthermore, the diminished H-bond interaction after adding PhSH is expected to be reflected in a back shift to low field. As shown in Figure 3a, the ^{31}P signal of the pure phosphate anion (−7.44 ppm; bottom) was shifted toward high field in the presence of the amide (−8.19 ppm; above), which is in full accordance with the previous results. However, upon addition of PhSH to the pure base, the phosphate signal was even further high field shifted to −8.69 ppm, which is in strong contrast to the ^{1}H spectra indicating only very weak H-bonds to PhSH in all thiol containing samples (*vide supra*). Thus, upon addition of PhSH another very strong H-bond has to be created independently of the thiol proton itself. This is also corroborated by the appearance of a ^{1}H signal at 16.43 ppm (PhSH: 3.94 ppm) for all PhSH/base containing mixtures. Since in our group dimers of chiral phosphoric acids were found to produce H-bond signals with ^{1}H chemical shifts around 16.00 ppm,[88] we suspected that a proton being H-bonded inside a phosphate dimer might cause this signal. Indeed, by adding a high excess of H_2O to the pure base in a control experiment, ^{1}H and ^{31}P signals at approximately equal

https://dx.doi.org/10.1021/jacs.0c08673
J. Am. Chem. Soc. 2021, 143, 724−735

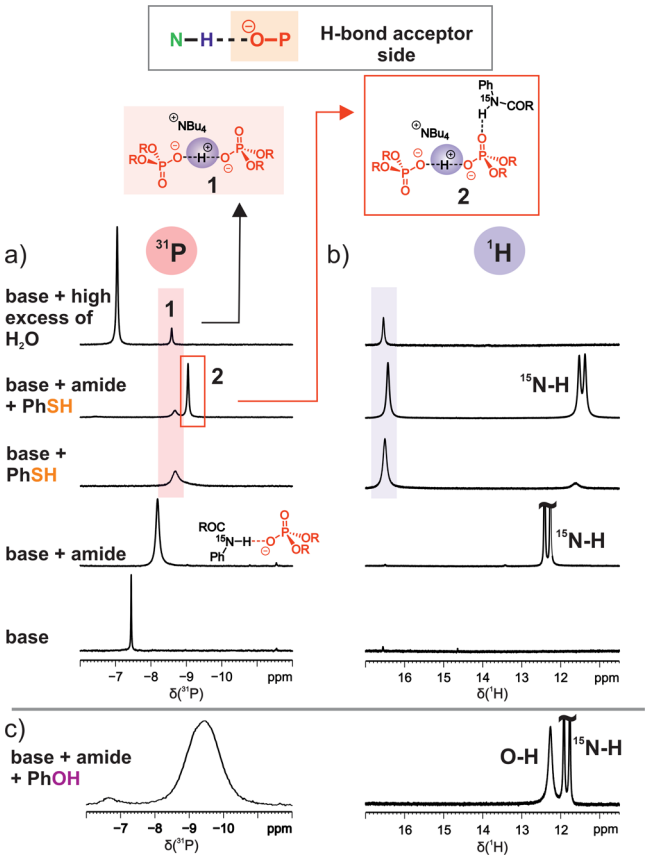

Figure 3. Phosphate dimer **1** possessing high electron density was identified as the crucial complex enabling strong H-bonds to amide: (a) The H-bond acceptor side was studied by ^{31}P NMR chemical shift analysis in CD_2Cl_2 at 180 K, and 1:1/1:1:1 mixtures were used for the multicomponent samples. For complete spectra, see SI. The high field shift of the phosphate after adding amide confirms the existence of an amide-base complex. Against the ^{1}H/^{15}N chemical shift trend (Figure 2c,d), the phosphate signal is further high field shifted in the presence of PhSH (red box). We assume dimer **1** is created by partial protonation of the base by PhSH (see SI chapter 4.1), which was also formed in a base/H_2O control experiment (top). The main signal (1:3 ratio) of the amide/base/PhSH mixture appeared at maximum high field position indicating high amounts of amide H-bonded in aggregate **2**. (b) The low field ^{1}H signals at ~16.5 ppm for PhSH containing as well as for the base/H_2O samples represent the hydrogen-bridged proton inside **1**. (c) The broad ^{31}P signal of the amide/base/PhOH sample corroborates a phenol containing large aggregate and the absence of dimer **1** is verified by ^{1}H NMR.

positions appeared (16.54/-8.59 ppm; Figure 3a, top), albeit in small concentrations. In addition, in mixtures of PhSH and base the occurrence of thiophenolate species was identified by NMR spectroscopy (a detailed characterization is given in chapter 4.1, SI). Thus, the addition of PhSH creates a new species, the phosphate dimer **1**, with a strong intermolecular P–O···H···O–P H-bond and high electron density being located at the ^{31}P nuclei identified by the high field shift. In the mixture of amide, base, and PhSH, the phosphate dimer **1** is present as well (see Figure 3a).

In addition, the main and sharper ^{31}P signal of the amide included complex is even further high field shifted (−9.05 ppm) indicating the highest electron density is located on the phosphate. This chemical shift reduction excludes a simple change in the concentration of the original amide–base complex and confirms a modulation of the overall aggregation. Therefore, the protonation of the phosphate by PhSH creates a classical network of phosphates H-bonded to both amide and phosphoric acid (N–H···A^-···H–A; with A being the phosphate). These structures could also be verified by MD simulations (*vide infra*). The higher electron density on the phosphates detected in these aggregates (see Figure 3a) indicates that a significant amount of phosphates is incorporated in extended H-bond networks with at least two H-bonds. The actual strengths of the N–H ···O–P H-bond is difficult to assess, since the DOSY experiments and the MD simulations discussed below show a release of the ammonium cations from the aggregate as well as a reduction of the overall amount of N–H moieties incorporated in H-bonds in the presence of phosphate dimers. In addition, an averaging of the chemical shifts with weaker bifurcated H-bond aggregates and/or a dynamic hopping of the amide from one phosphate to the other within dimer **1** may occur. Such proton exchange on the NMR time scale is corroborated by the line broadening of the N–H proton in the ^{1}H NMR spectrum (Figure 2c, top). The bifurcation motif could directly be found in our MD derived snapshots (*vide infra*). Nevertheless, the interaction of the phosphate dimers with the amides and the resulting change of the overall aggregation is clearly visible from the ^{31}P spectra.

In contrast, for the amide/base/phenol mixture only a very broad ^{31}P signal over a ppm region of −7.77 to −11.16 ppm was detected but no ^{1}H signal at around 16.50 ppm (see Figure 3c). This indicates no protonation of phosphate and in consequence no phosphate dimer formation with phenol in accordance with the relative pK_a values of thiophenol and phenol (pK_a (PhSH): 10; pK_a (PhOH): 18; in DMSO).[92] The high field position of the base signal indicates high electron density also for this complex potentially induced by extended networks with phenol.

The presented data show that thiophenol is able to partially protonate the phosphate in an acid–base reaction and to form H-bond mediated P–O···H···O–P dimers, while with phenol as the additive no phosphate protonation occurs. However, the ^{1}H and ^{31}P chemical shifts as average parameters of the H-bond strengths are similar in both cases. This is an indication that besides H-bond strengths also the overall molecular arrangement is important for reactivity.

Aggregation Analysis by NMR. Therefore, the nature of the different aggregates was analyzed in detail via diffusion ordered spectroscopy (DOSY) at 300 and 180 K. From the obtained self-diffusion coefficients, which refer to averaged values for the species in the entire solution, the viscosity corrected volumes V (DOSY) were calculated (for details see SI chapter 4.6.2). In Figure 4, the volumes derived from DOSY for the amide/base, amide/base/PhSH, and the amide/base/PhOH mixtures as well as the literature derived monomer volumes according to Bondi[93] are summarized.

At both temperatures large aggregates were detected as expected for ion pairs and molecules (amides), which can form H-bonds in apolar organic solvents. The modulation of aggregation between ambient and low temperature follows the expected trends. The amide tends toward higher aggregates at 180 K, while the ion pair shows higher complexation at room temperature due to the reduced dielectric constant of the solvent (see Figure 4 and Table S1, SI).

However, at both temperatures the high amount of aggregation exemplifies that it is of utmost importance for the interpretation of H-bond networks in PCET reactions to check the aggregation situation at the concentrations used in

https://dx.doi.org/10.1021/jacs.0c08673
J. Am. Chem. Soc. 2021, 143, 724–735

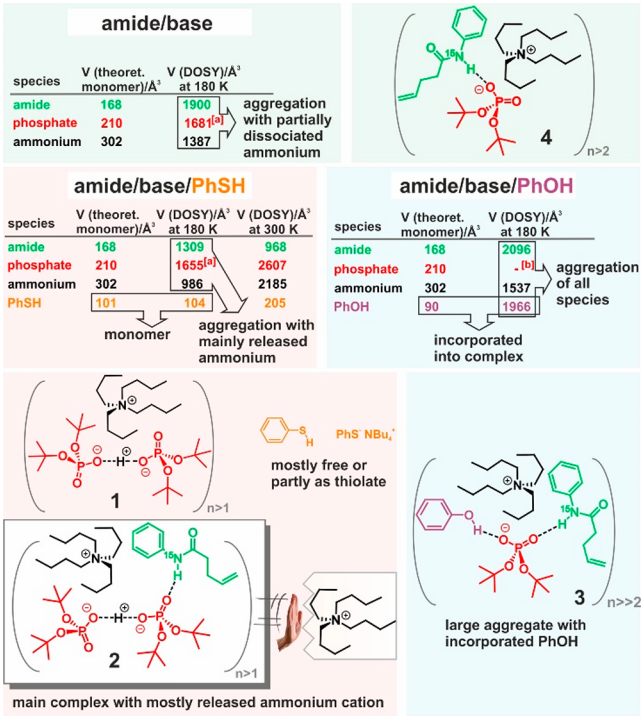

Figure 4. Reduced aggregation in the presence of PhSH and release of ammonium: An overview of the main aggregates identified by ^{1}H, ^{15}N, ^{31}P NMR, DOSY, and MD simulations is given. The tables summarize the DOSY derived volumes and the estimated van der Waals monomer values according to Bondi.[93] Large amide-base aggregation (top) shown as complex **4** with partial release of the ammonium counterion was identified. In addition to dimer **1** the main amide containing aggregate **2** with mostly released counterion and an immense disaggregation was identified for the PhSH containing mixture. In contrast, for the amide/base/PhOH sample, the volumes verify the formation of a large PhOH containing aggregate **3**. [a]The value is assumed to be higher, as the phosphate signal is not completely baseline separated from the adjacent ammonium CH_2 groups. [b]Complete overlap of signals made the analysis of the phosphate diffusion impossible.

catalysis and not in highly diluted samples usually used for UV luminescence quenching.

Amide/Base and Amide/Base/Thiophenol. In the following only the aggregation at low temperature is discussed, as this can be analyzed by both H-bond study and MD simulations. For the amide/base sample, large volumes were obtained for both the amide (V(DOSY) = 1900 Å^3) and phosphate (V(DOSY) = 1681 Å^3) confirming the existence of an amide−base complex, proposed as aggregate **4** (Figure 4).[94] The low volume of NBu_4^+ indicates (V(DOSY) = 1389 Å^3) a partial dissociation from complex **4**. In the presence of PhSH, surprisingly, an immense reduction of the amide complexation was obtained (ΔV(DOSY) = 591 Å^3). This suggests less self-aggregation and partial release of the substrate from the phosphate complex. This unexpected result also explains the reduction of the ^{1}H and ^{15}N chemical shifts after addition of PhSH. Due to the low time resolution of NMR spectroscopy, the signals of the highly activated N−H moieties in H-bonds with the P−O···H···O−P dimers are averaged with non-activated N−H moieties of pure amides and the real activation is masked by the crowd of aggregates. Only in the nonaveraged signal of the phosphate−amide interaction the extended H-bond network is reflected. In addition, the comparably small DOSY derived value of NBu_4^+ (V = 986 Å^3) indicates that upon addition of PhSH even a higher percentage of the cation is pushed away from the phosphate complex, which may support higher electron densities on phosphate as well. Of course, also the formation of thiolate−NBu_4^+ complexes may explain the small volumes to some extent. For the pure PhSH, the volume is within the range of the monomer, which is in full accordance with the poor H-bond donor ability.

Amide/Phosphate/Phenol. In contrast, the measurement of the amide/base/phenol sample yielded immense values for both the amide and phenol species (V(DOSY) = 2096 and 1966 Å^3). Thus, both compounds are incorporated in large aggregates (see aggregate **3** in Figure 4). As a result, the amide−phosphate and the phenol−phosphate H-bonds coexist competitively in large ensembles. The reduced activity using PhOH for the hydroamidation indicates that both H-bond competition and aggregation are potentially detrimental to reactivity as was shown for aggregation in flavin photocatalysis.[95]

These data show that PhSH generates a phosphate dimer with increased electron density and a H-bond network to amides within smaller aggregates, which partially release ammonium cations while phenol produces larger aggregates with H-bonds, which are competitive to those of the amide.

Molecular-Dynamics (MD) Simulations. In order to obtain more details about the essential substrate activating aggregates, MD simulations were performed. While the underlying classical force fields often require care for quantitative predictions of solution structures, they can give a qualitative account of the manifold of expected and unexpected aggregates that are present in complex mixed solutions. In Figure 5, selected PCET relevant snapshots of a simulation containing *N*-phenylpent-4-enamide, a di-*tert*-butyl phosphate anion, a tetrabutylammonium cation, thiophenolate, *tert*-butyl phosphoric acid, H_2O, and H_3O^+ are depicted. The acid was used in order to be able to mimic the phosphate−H^+ interaction. For detailed information about the simulations, see chapter 5 in the SI. In general, the existence of phosphate dimer **1** was verified. The crucial complex **2**, which is formed via attachment of the amidyl N−H group to the phosphate dimer, could also be directly found (Figure 5; top). In

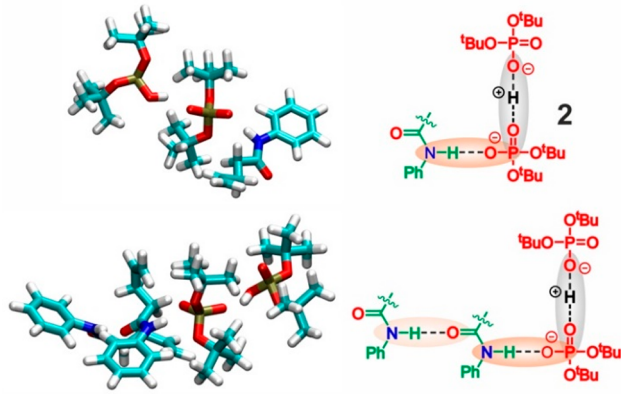

Figure 5. The PCET relevant amide containing aggregate **2** was verified by MD simulations: MD snapshots of a mixture containing *N*-phenylpent-4-enamide, di-*tert*-butyl phosphate anion, tetrabutylammonium cation, *tert*-butyl phosphoric acid, thiophenolate, H_2O, and H_3O^+ show the H-bond mediated amide-dimer complex **2** (top) and an additional extended H-bond motif with two amides (bottom).

https://dx.doi.org/10.1021/jacs.0c08673
J. Am. Chem. Soc. 2021, 143, 724−735

addition, hydrogen bridged to this complex by N−H···O═C, a second amide was found to contribute to the extended H-bond network in a cooperative way. Also sterically demanding complexes with one amide attached to the phosphate and one on the phosphoric acid of dimer **1** could be detected, which showed geometrically distorted, i.e. weaker, H-bonds (see Scheme S59). Furthermore, a significant reduction of the absolute number of H-bonds between amide and phosphate was calculated upon addition of PhSH.

Considering the averaging function of the ensemble, these findings explain the overall reduction of the amide−phosphate H-bond strength in the presence of PhSH indicated by the $^{1}H/^{15}N$ high field shift of the $^{15}N-H$ doublet representing all amide-containing species inside the solution. Thus, also the MD simulations corroborate significant changes of the overall aggregates in the presence of protons originating from the acidic channel of thiophenol.[96]

Multisite Effect of PhSH within the Mechanism. The mechanism of the photocatalyzed hydroamidation is extremely complex, and the PhSH additive can act both as an acid and as a radical. Therefore, the presence of PhSH has an impact on multiple rates at different stages of the reaction (see violet boxes for proton channels and gray boxes for radical channels of PhSH in Figure 6). The protonated phosphate dimers

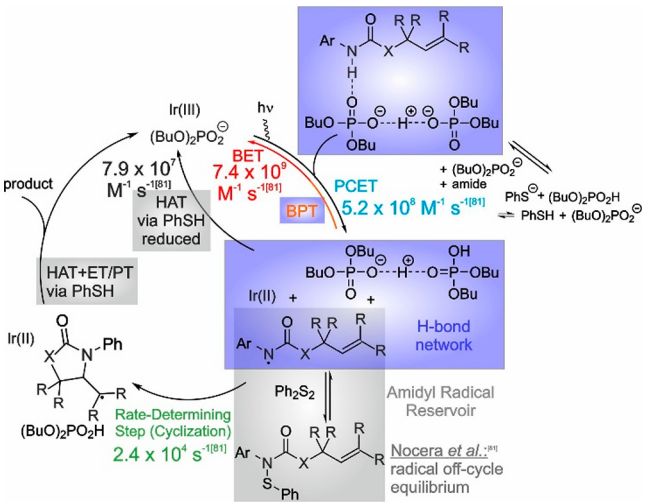

Figure 6. Multisite effects of PhSH on the mechanism in hydroamidation reactions. Mechanistic steps affected by the acidic properties of PhSH are highlighted with violet boxes, those affected by the radical properties with gray boxes. Ionic and radical channels are intertwined via the partial deprotonation of PhSH. The rates presented originate from previous studies by Nocera and co-workers.[81]

themselves and the resulting aggregates discussed above can influence the initial PCET step as well as the BPT via potential proton trapping and/or differences in their aggregate size. PhSH as the radical may impact the radical off-cycle equilibrium as well as the two HAT steps. In addition, the amount of thiolate anions reduces the availability of PhSH for the radical channels; thus, the radical and ionic channel intertwine. Therefore, PhSH and its derivatives were regarded as unfavorable additives to separate these effects and additives were selected which allow for separating the radical and the ionic pathways at least in the ground state.

Acceleration Effects Substituting PhSH by Diphenyldisulfide and Phosphoric Acid. In case the radical and the ionic pathway influence the hydroamidation reaction independently from each other, it should be possible to replace the radical part of PhSH and the acidic part by two additives. Given the complex mechanism shown in Figure 6, it is key for further understanding to avoid additional players in the cycle. Therefore, Ph_2S_2 was selected to represent the radical part of PhSH and phosphoric acid was chosen to replace the acidic part of PhSH. Both Ph_2S_2 and phosphoric acid were detected by NMR in the reaction mixtures with PhSH as the exclusive additive. This separation of the properties of PhSH into two additives opens the unique opportunity to modulate the relative amount of acid and radicals by using different ratios.[97]

Indeed, the initial rate kinetics of amide, Ph_2S_2, and different mixtures of phosphate and phosphoric acid show that the addition of acid accelerates the photoredox catalytic reaction (Figure 7) up to three times, which is even higher than the

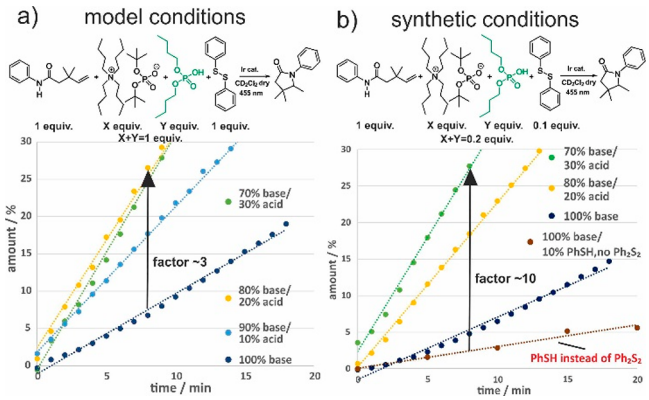

Figure 7. Acceleration effects substituting PhSH by phosphoric acid and Ph_2S_2 presented by initial rate kinetics of amide, Ph_2S_2, and different amounts of base and acid; (a) in 1:1:1 mixtures of amide/Ph_2S_2/acid+base acceleration effects up to a factor of 3 validate the effect of the proton network on the photoredox catalytic reaction; (b) under synthetic conditions (1:0.1:0.2 of amide/Ph_2S_2/acid+base) the selective optimization of ionic and radical channels allows even an acceleration by 1 order of magnitude.

acceleration effect of PhSH with its partially acidic function (see Figure 2a, top; di-*n*-butyl phosphoric acid was used because of instability of the *tert*-butyl acid).

In addition, again the proton signature of the phosphate dimer was detected, corroborating the assignment (see Figure S26). Under synthetic reaction conditions the acceleration effect is even more pronounced (see Figure 7b). Compared to the reaction with base and disulfide only the real reaction is accelerated up to a factor of ∼4 (the values are derived from the comparison of the slopes; see chapter 3.6 and 3.7 in the SI). Compared to the initially published reaction conditions in the presence of PhSH (see Figure 2a, bottom, and brown curve in Figure 7b) even a factor of ∼10 is achieved.[32] As a result, these mechanistic investigations show that the radical and the acidic properties of PhSH can be successfully replaced by a combination of disulfide and acid. In addition, by applying these two additives, the radical and the acidic properties can be selectively modulated and optimized leading to a reactivity improvement of 1 order of magnitude. We expect that this will have a huge impact on the developments in synthetic chemistry.

https://dx.doi.org/10.1021/jacs.0c08673
J. Am. Chem. Soc. 2021, 143, 724−735

Effect of Phosphoric Acid on the Mechanism. Next, we investigated which steps in the mechanism contribute to the observed acceleration upon addition of phosphoric acid. First, the effect of the proton network on the photoreaction was tested via luminescence quenching experiments at relevant synthetic concentrations (for details, see chapter 6, SI). Previous studies determined very fast and highly effective PCET rates close to the diffusion limit.[80,81] Indeed, the emission decays of the excited photocatalyst were fastest without acid as the additive (see Figure S62). The luminescence decays show that addition of phosphoric acid significantly slows down the quenching of the photocatalyst's excited state, as expected for quenching species becoming bulkier with increasing amounts of acid. This is in agreement with DOSY measurements showing larger aggregates in the presence of phosphoric acid (see Table S1) and excludes the photostep effecting the acceleration of the overall reaction (for mechanistic scheme, see Figure 8a). Since acid slows down the PCET step, the observed acceleration can be caused by either an acceleration of the productive radical cyclization or a reduction of the unproductive BET/BPT back reaction.

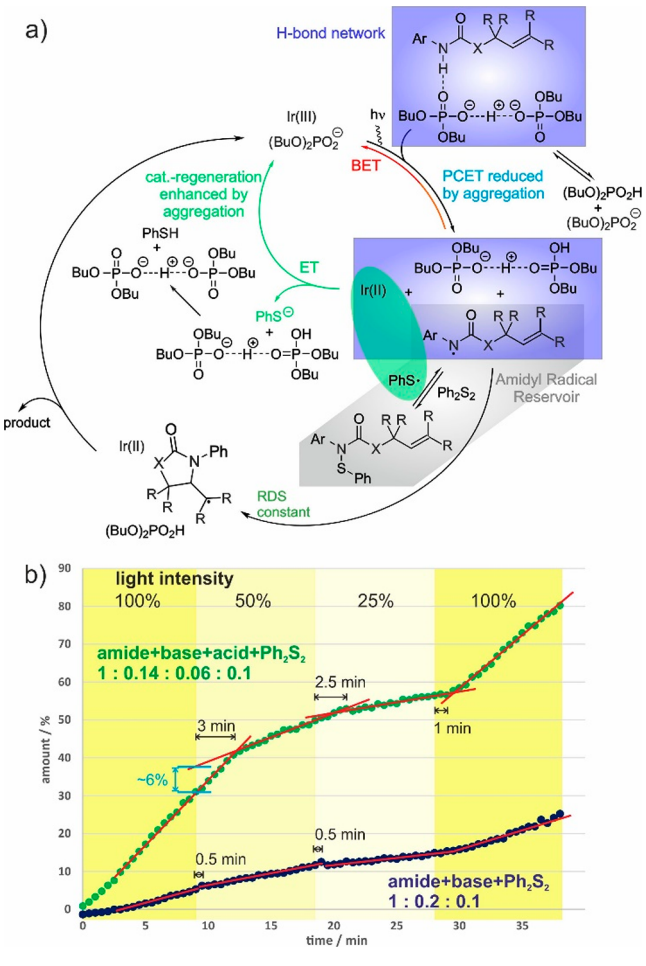

Figure 8. (a) Mechanistic proposal using Ph_2S_2 and phosphoric acid instead of PhSH; (b) light intensity dependent reaction profiles reflecting conditions of a mixture of amide/base/Ph_2S_2 (blue curve) and a mixture of amide, base+acid (70:30), and Ph_2S_2 (green curve). The observed persistence times after reducing the light intensity indicate a large amidyl radical reservoir in the presence of acid. This as well as the light intensity dependent persistence times reveal a productive pathway of regenerating Ir(III). For details, see text.

Therefore, next the availability of the photogenerated amidyl radical was tested, which is the key intermediate for the productive reaction. We achieved this by measuring NMR reaction profiles, applying different light intensities during the reaction (see Figure 8b). The exclusive change of light intensity allows the different steps in the mechanism regarding the amount of amidyl radical to be dissected. The PCET generation of the radical should be proportional to the light intensity. The rate constant of the cyclization step should be independent of the light intensity and constant at least within one reaction profile. As a result, the rate of the cyclization, which can be read out in the slope of the overall reaction profile is expected to be proportional to the amount of photogenerated amidyl radical available for the productive reaction.

The blue curve in Figure 8b shows the response of the overall reaction with disulfide and base. After reducing the light intensity to 50% or to 25%, a small persistence of the previous reaction rate is observed for about half a minute. An acceleration of the cyclization should reduce the amount of the photogenerated amidyl radical. In contrast the reduction of the BET/BPT should increase the amount of the amidyl radical intermediate.

This is in contrast to our previous studies, in which direct responses to light reduction were detected (upon light reduction the systems relaxed below the NMR time resolution to the new photochemical equilibrium situation even in the case of reaction intermediates).[98] This indicates the formation of an amidyl reservoir feeding the cyclization over a longer time span. Such an accumulation of the amidyl radical photogenerated at higher light intensity in the presence of Ph_2S_2 is in agreement with the mechanistic proposal and the relative reaction rates previously proposed by Nocera and co-workers (see Figure 6), in which the amidyl radical is stored as the S−N intermediate shown in Figure 8.[81] Thus, in the following the term amidyl radical reservoir describes both the amidyl radical itself and the amidyl radical stored in this S−N intermediate. The PCET step is very fast, while the amidyl cyclization is the rate-determining step of the reaction. In case the BET/BPT back reaction can be slowed down, an excess formation of amidyl radical is expected. This was achieved by Ph_2S_2 as the additive providing an off-cycle equilibrium to the S−N intermediate. This amidyl reservoir seems to be now visible in the persisting slope corresponding to the preceding light intensity (and in the slower initial buildup in the first minutes, see also Figure 7). In principle, different times for this persistence of the slope depending on the preceding light intensity are expected; however, the slow time resolution of the NMR spectra (0.5 min per spectrum) is not sufficient in the case of Ph_2S_2 as the exclusive additive.

Upon applying a 30:70 mixture of phosphoric acid and base, again a significant acceleration at 100% light was observed. After reducing the light to 50% intensity, a persistence of the initial reaction rate over 3 min can be observed (green curve in Figure 8b). This directly shows that, with acid as the additive, a significantly larger amidyl reservoir is formed. In addition, this indirectly proves the presence of the S−N intermediate, since the pure amidyl radical would be consumed by far faster by the cyclization reaction (2.4×10^4 s^{-1}).[81] By reducing the light intensity from 50% to 25%, this persistence of the previous rate is repeated but the length is shorter (2.5 min) as anticipated for lower light intensities. This pattern is corroborated by the third switching of the light intensity: Again, the previous slope

https://dx.doi.org/10.1021/jacs.0c08673
J. Am. Chem. Soc. 2021, 143, 724−735

continues, but for a shorter time. These data show that with acid such a huge excess of amidyl radical is formed (and stored in the S−N intermediate) and that even the slow time resolution of NMR spectroscopy is sufficient to resolve the additive-dependent offset between the photogenerated formation of an amidyl radical reservoir and its reaction in the downstream dark reaction.

After reduction of the light from 100% to 50%, around 10% conversion is observed at the initial rate, which is significantly more than the 2% of Ir(III) catalyst available in this reaction (even in case the ongoing conversion at 50% is subtracted). This substantial size of the amidyl reservoir indicates that a productive regeneration pathway of Ir(II) to Ir(III) has to be present prior to the cyclization reaction. Initially this regeneration was proposed by Knowles and co-workers via a sequential ET/PT involving PhS· and phosphoric acid after the cyclization step (see Figure 1b). Considering the off-cycle equilibrium to the S−N intermediate creating PhS· and the presence of additional protons in close proximity within the phosphate dimers, we propose this additional Ir(III) regeneration pathway directly after the PCET step as shown in Figure 8a.

In principle, this shortcut should be also possible in the presence of disulfide and without additional acid since phosphoric acid is generated in the PCET step and PhS· is available from the off-cycle equilibrium to the S−N intermediate. However, the reaction profiles only with disulfide in Figure 8b show only a very short persistence of the previous reaction rate upon light reduction. In contrast, with 30% acid a persistence up to 3 min is observed. This shows clearly the importance of additional protons, which are in close proximity (phosphate dimers) to the reaction center which is key to an effective and productive regeneration of the reduced Ir(II) catalyst back to the initial Ir(III) state.

Overall, reaction profiles with variation of the light intensity are used to dissect the effect of acid on the different mechanistic steps within the catalytic cycle. In the presence of acid, persistence times of the reaction rate at higher light intensities were observed over minutes after attenuating the light, indicating the formation of a large amidyl radical reservoir. This shows that additional protons in close proximity are able to open up a productive shortcut for the photocatalyst regeneration prior to the slow cyclization step.

CONCLUSION

In conclusion, this study shows that complex aggregation and H-bond networks are potentially present under synthetic conditions in photoredox catalysis, which affect key properties in terms of reactivity. Due to highly diluted samples in many UV studies, these effects have been often overlooked so far. Regarding the puzzling activation effect of thiophenol in PCET hydroamidation reactions, it was shown that the interplay of sophisticated NMR studies, MD simulations, initial rate kinetics, and light-dependent reaction profiles allow the disclosure of activation patterns which are hidden by the average properties of the ensembles.

To our knowledge, the combination of techniques within this study reveals quite a number of aspects in photocatalysis for the first time: (1) An extended H-bond network was directly detected as the key element in photocatalysis, here allowing a productive shortcut for the regeneration of the reduced photocatalyst to become effective. (2) The broadly used PhSH additive in photocatalysis was shown to be replaceable by disulfide and acid, allowing for the first time an individual tuning of the radical and ionic channel and yielding accelerations up to a factor of ∼10 under synthetic conditions. (3) Advanced NMR studies in combination with MD-simulations revealed activation modes of photoredox catalysis within a complex ensemble of H-bond assisted ion pairs. (4) Light intensity dependent reaction profiles allowed the accumulation of a photogenerated radical species to be traced indirectly and the correlation of the overall reaction rate to individual mechanistic steps.

We expect that all aspects of this study, ensembles and extended H-bond networks, proton transfer pathways, and tuning of ionic and radical channels, will play crucial roles in future photoredox catalysis.

ASSOCIATED CONTENT

Supporting Information

The Supporting Information is available free of charge at https://pubs.acs.org/doi/10.1021/jacs.0c08673.

Detailed experimental procedures, sample preparation, NMR spectroscopic data, MD simulation and emission experiments (PDF)

AUTHOR INFORMATION

Corresponding Author

Ruth M. Gschwind − *Institute of Organic Chemistry, University of Regensburg, D-93053 Regensburg, Germany;* orcid.org/0000-0003-3052-0077; Email: ruth.gschwind@chemie.uni-regensburg.de

Authors

Nele Berg − *Institute of Organic Chemistry, University of Regensburg, D-93053 Regensburg, Germany*

Sebastian Bergwinkl − *Institute of Physical and Theoretical Chemistry, University of Regensburg, D-93053 Regensburg, Germany*

Patrick Nuernberger − *Institute of Physical and Theoretical Chemistry, University of Regensburg, D-93053 Regensburg, Germany;* orcid.org/0000-0002-4690-0229

Dominik Horinek − *Institute of Physical and Theoretical Chemistry, University of Regensburg, D-93053 Regensburg, Germany;* orcid.org/0000-0002-0958-0043

Complete contact information is available at: https://pubs.acs.org/10.1021/jacs.0c08673

Notes

The authors declare no competing financial interest.

ACKNOWLEDGMENTS

We thank the German Science Foundation (DFG; GRK 1626 Chemical Photocatalysis; GRK 2620 Ion Pair Effects) for financial and intellectual support.

REFERENCES

(1) Huynh, M. H. V.; Meyer, T. J. Proton-Coupled Electron Transfer. *Chem. Rev.* **2007**, *107* (11), 5004−5064.

(2) Weinberg, D. R.; Gagliardi, C. J.; Hull, J. F.; Murphy, C. F.; Kent, C. A.; Westlake, B. C.; Paul, A.; Ess, D. H.; McCafferty, D. G.; Meyer, T. J. Proton-Coupled Electron Transfer. *Chem. Rev.* **2012**, *112* (7), 4016−4093.

(3) Kaila, V. R. I.; Verkhovsky, M. I.; Wikström, M. Proton-Coupled Electron Transfer in Cytochrome Oxidase. *Chem. Rev.* **2010**, *110* (12), 7062−7081.

(4) Reece, S. Y.; Nocera, D. G. Proton-Coupled Electron Transfer in Biology: Results from Synergistic Studies in Natural and Model Systems. *Annu. Rev. Biochem.* **2009**, *78* (1), 673−699.
(5) Migliore, A.; Polizzi, N. F.; Therien, M. J.; Beratan, D. N. Biochemistry and Theory of Proton-Coupled Electron Transfer. *Chem. Rev.* **2014**, *114* (7), 3381−3465.
(6) Weinberg, D. R.; Gagliardi, C. J.; Hull, J. F.; Murphy, C. F.; Kent, C. A.; Westlake, B. C.; Paul, A.; Ess, D. H.; McCafferty, D. G.; Meyer, T. J. Proton-Coupled Electron Transfer. *Chem. Rev.* **2012**, *112*, 4016.
(7) Meyer, T. J.; Huynh, M. H. V.; Thorp, H. H. The Possible Role of Proton-Coupled Electron Transfer (PCET) in Water Oxidation by Photosystem II. *Angew. Chem., Int. Ed.* **2007**, *46* (28), 5284−5304.
(8) Stubbe, J.; Nocera, D. G.; Yee, C. S.; Chang, M. C. Y. Radical Initiation in the Class I Ribonucleotide Reductase: Long-Range Proton-Coupled Electron Transfer? *Chem. Rev.* **2003**, *103* (6), 2167−2202.
(9) Hatcher, E.; Soudackov, A. V.; Hammes-Schiffer, S. Proton-Coupled Electron Transfer in Soybean Lipoxygenase. *J. Am. Chem. Soc.* **2004**, *126* (18), 5763−5775.
(10) Wang, Y.; Chen, H.; Makino, M.; Shiro, Y.; Nagano, S.; Asamizu, S.; Onaka, H.; Shaik, S. Theoretical and Experimental Studies of the Conversion of Chromopyrrolic Acid to an Antitumor Derivative by Cytochrome P450 StaP: The Catalytic Role of Water Molecules. *J. Am. Chem. Soc.* **2009**, *131* (19), 6748−6762.
(11) Bonin, J.; Robert, M. Photoinduced Proton-Coupled Electron Transfers in Biorelevant Phenolic Systems. *Photochem. Photobiol.* **2011**, *87* (6), 1190−1203.
(12) Kaila, V. R. I. Long-Range Proton-Coupled Electron Transfer in Biological Energy Conversion: Towards Mechanistic Understanding of Respiratory Complex I. *J. R. Soc., Interface* **2018**, *15* (141), 20170916.
(13) Mora, S. J.; Odella, E.; Moore, G. F.; Gust, D.; Moore, T. A.; Moore, A. L. Proton-Coupled Electron Transfer in Artificial Photosynthetic Systems. *Acc. Chem. Res.* **2018**, *51* (2), 445−453.
(14) Tommos, C.; Babcock, G. T. Oxygen Production in Nature: A Light-Driven Metalloradical Enzyme Process. *Acc. Chem. Res.* **1998**, *31* (1), 18−25.
(15) Costentin, C.; Robert, M.; Savéant, J.-M. Electrochemical Approach to the Mechanistic Study of Proton-Coupled Electron Transfer. *Chem. Rev.* **2010**, *110* (12), 2145−2179.
(16) Madhiri, N.; Finklea, H. O. Potential-, PH-, and Isotope-Dependence of Proton-Coupled Electron Transfer of an Osmium Aquo Complex Attached to an Electrode. *Langmuir* **2006**, *22* (25), 10643−10651.
(17) Hammes-Schiffer, S.; Soudackov, A. V. Proton-Coupled Electron Transfer in Solution, Proteins, and Electrochemistry. *J. Phys. Chem. B* **2008**, *112* (45), 14108−14123.
(18) Hammes-Schiffer, S. Proton-Coupled Electron Transfer: Moving Together and Charging Forward. *J. Am. Chem. Soc.* **2015**, *137* (28), 8860−8871.
(19) Ghosh, S.; Soudackov, A. V.; Hammes-Schiffer, S. Electrochemical Electron Transfer and Proton-Coupled Electron Transfer: Effects of Double Layer and Ionic Environment on Solvent Reorganization Energies. *J. Chem. Theory Comput.* **2016**, *12* (6), 2917−2925.
(20) Savéant, J. M. Electrochemical Approach to Proton-Coupled Electron Transfers: Recent Advances. *Energy Environ. Sci.* **2012**, *5* (7), 7718−7731.
(21) Costentin, C.; Savéant, J. M. Theoretical and Mechanistic Aspects of Proton-Coupled Electron Transfer in Electrochemistry. *Curr. Opin. Electrochem.* **2017**, *1* (1), 104−109.
(22) Savéant, J.-M. Concerted Proton-Electron Transfers: Fundamentals and Recent Developments. *Annu. Rev. Anal. Chem.* **2014**, *7* (1), 537−560.
(23) Costentin, C.; Robert, M.; Savéant, J. M.; Tard, C. Breaking Bonds with Electrons and Protons. Models and Examples. *Acc. Chem. Res.* **2014**, *47* (1), 271−280.
(24) Li, B.; Zhao, J.; Onda, K.; Jordan, K. D.; Yang, J.; Petek, H. Ultrafast Interfacial Proton-Coupled. *Science* **2006**, *311* (March), 1436−1440.
(25) Symes, M. D.; Surendranath, Y.; Lutterman, D. A.; Nocera, D. G. Bidirectional and Unidirectional PCET in a Molecular Model of a Cobalt-Based Oxygen-Evolving Catalyst. *J. Am. Chem. Soc.* **2011**, *133* (14), 5174−5177.
(26) Costentin, C.; Drouet, S.; Robert, M.; Saveant, J.-M. A Local Proton Source Enhances CO2 Electroreduction to CO by a Molecular Fe Catalyst. *Science* **2012**, *338* (6103), 90−94.
(27) Markle, T. F.; Darcy, J. W.; Mayer, J. M. A New Strategy to Efficiently Cleave and Form C−H Bonds Using Proton-Coupled Electron Transfer. *Sci. Adv.* **2018**, *4* (7), eaat5776.
(28) Liu, T.; Guo, M.; Orthaber, A.; Lomoth, R.; Lundberg, M.; Ott, S.; Hammarström, L. Accelerating Proton-Coupled Electron Transfer of Metal Hydrides in Catalyst Model Reactions. *Nat. Chem.* **2018**, *10* (8), 881−887.
(29) Fava, E.; Nakajima, M.; Nguyen, A. L. P.; Rueping, M. Photoredox-Catalyzed Ketyl-Olefin Coupling for the Synthesis of Substituted Chromanols. *J. Org. Chem.* **2016**, *81* (16), 6959−6964.
(30) Lefebvre, Q.; Hoffmann, N.; Rueping, M. Photoorganocatalysed and Visible Light Photoredox Catalysed Trifluoromethylation of Olefins and (Hetero)Aromatics in Batch and Continuous Flow. *Chem. Commun.* **2016**, *52* (12), 2493−2496.
(31) Choi, G. J.; Knowles, R. R. Catalytic Alkene Carboaminations Enabled by Oxidative Proton-Coupled Electron Transfer. *J. Am. Chem. Soc.* **2015**, *137* (29), 9226−9229.
(32) Miller, D. C.; Choi, G. J.; Orbe, H. S.; Knowles, R. R. Catalytic Olefin Hydroamidation Enabled by Proton-Coupled Electron Transfer. *J. Am. Chem. Soc.* **2015**, *137* (42), 13492−13495.
(33) Choi, G. J.; Zhu, Q.; Miller, D. C.; Gu, C. J.; Knowles, R. R. Catalytic Alkylation of Remote C−H Bonds Enabled by Proton-Coupled Electron Transfer. *Nature* **2016**, *539* (7628), 268−271.
(34) Rono, L. J.; Yayla, H. G.; Wang, D. Y.; Armstrong, M. F.; Knowles, R. R. Enantioselective Photoredox Catalysis Enabled by Proton-Coupled Electron Transfer: Development of an Asymmetric Aza-Pinacol Cyclization. *J. Am. Chem. Soc.* **2013**, *135* (47), 17735−17738.
(35) Yayla, H. G.; Wang, H.; Tarantino, K. T.; Orbe, H. S.; Knowles, R. R. Catalytic Ring-Opening of Cyclic Alcohols Enabled by PCET Activation of Strong O−H Bonds. *J. Am. Chem. Soc.* **2016**, *138* (34), 10794−10797.
(36) Miller, D. C.; Tarantino, K. T.; Knowles, R. R. Proton-Coupled Electron Transfer in Organic Synthesis: Fundamentals, Applications and Opportunities. *Top. Curr. Chem.* **2016**, *374* (3), 1−59.
(37) Gentry, E. C.; Knowles, R. R. Synthetic Applications of Proton-Coupled Electron Transfer. *Acc. Chem. Res.* **2016**, *49* (8), 1546−1556.
(38) Yayla, H. G.; Knowles, R. R. Proton-Coupled Electron Transfer in Organic Synthesis: Novel Homolytic Bond Activations and Catalytic Asymmetric Reactions with Free Radicals. *Synlett* **2014**, *25* (21), 2819−2826.
(39) Qiu, G.; Knowles, R. R. Rate−Driving Force Relationships in the Multisite Proton-Coupled Electron Transfer Activation of Ketones. *J. Am. Chem. Soc.* **2019**, *141* (6), 2721−2730.
(40) Hoffmann, N. Proton-Coupled Electron Transfer in Photoredox Catalytic Reactions. *Eur. J. Org. Chem.* **2017**, *2017* (15), 1982−1992.
(41) Nguyen, L. Q.; Knowles, R. R. Catalytic C−N Bond-Forming Reactions Enabled by Proton-Coupled Electron Transfer Activation of Amide N−H Bonds. *ACS Catal.* **2016**, *6* (5), 2894−2903.
(42) Tarantino, K. T.; Liu, P.; Knowles, R. R. Catalytic Ketyl-Olefin Cyclizations Enabled by Proton-Coupled Electron Transfer. *J. Am. Chem. Soc.* **2013**, *135* (27), 10022−10025.
(43) Zhu, Q.; Graff, D. E.; Knowles, R. R. Intermolecular Anti-Markovnikov Hydroamination of Unactivated Alkenes with Sulfonamides Enabled by Proton-Coupled Electron Transfer. *J. Am. Chem. Soc.* **2018**, *140*, 741−747.
(44) Ota, E.; Wang, H.; Frye, N. L.; Knowles, R. R. A Redox Strategy for Light-Driven, Out-of-Equilibrium Isomerizations and Application

https://dx.doi.org/10.1021/jacs.0c08673
J. Am. Chem. Soc. 2021, 143, 724−735

to Catalytic C-C Bond Cleavage Reactions. *J. Am. Chem. Soc.* **2019**, *141*, 1457.
(45) Wenger, O. S. Proton-Coupled Electron Transfer with Photoexcited Metal Complexes. *Acc. Chem. Res.* **2013**, *46* (7), 1517−1526.
(46) Hammes-Schiffer, S.; Stuchebrukhov, A. A. Theory of Coupled Electron and Proton Transfer Reactions. *Chem. Rev.* **2010**, *110* (12), 6939−6960.
(47) Mayer, J. M.; Rhile, I. J. Thermodynamics and Kinetics of Proton-Coupled Electron Transfer: Stepwise vs. Concerted Pathways. *Biochim. Biophys. Acta, Bioenerg.* **2004**, *1655* (1−3), 51−58.
(48) Zhao, K.; Yamashita, K.; Carpenter, J. E.; Sherwood, T. C.; Ewing, W. R.; Cheng, P. T. W.; Knowles, R. R. Catalytic Ring Expansions of Cyclic Alcohols Enabled by Proton-Coupled Electron Transfer. *J. Am. Chem. Soc.* **2019**, *141* (22), 8752−8757.
(49) Nguyen, S. T.; Zhu, Q.; Knowles, R. R. PCET-Enabled Olefin Hydroamidation Reactions with N-Alkyl Amides. *ACS Catal.* **2019**, *9* (5), 4502−4507.
(50) Morton, C. M.; Zhu, Q.; Ripberger, H.; Troian-Gautier, L.; Toa, Z. S. D.; Knowles, R. R.; Alexanian, E. J. C−H Alkylation via Multisite-Proton-Coupled Electron Transfer of an Aliphatic C−H Bond. *J. Am. Chem. Soc.* **2019**, *141* (33), 13253−13260.
(51) Wang, D.; Loose, F.; Chirik, P. J.; Knowles, R. R. N−H Bond Formation in a Manganese(V) Nitride Yields Ammonia by Light-Driven Proton-Coupled Electron Transfer. *J. Am. Chem. Soc.* **2019**, *141* (12), 4795−4799.
(52) Shin, N. Y.; Ryss, J. M.; Zhang, X.; Miller, S. J.; Knowles, R. R. Light-Driven Deracemization Enabled by Excited-State Electron Transfer. *Science* **2019**, *366*, 364−369.
(53) Bissonnette, N. B.; Ellis, J. M.; Hamann, L. G.; Romanov-Michailidis, F. Expedient Access to Saturated Nitrogen Heterocycles by Photoredox Cyclization of Imino-Tethered Dihydropyridines. *Chem. Sci.* **2019**, *10* (41), 9591−9596.
(54) Caron, A.; Morin, É.; Collins, S. K. Bifunctional Copper-Based Photocatalyst for Reductive Pinacol-Type Couplings. *ACS Catal.* **2019**, *9* (10), 9458−9464.
(55) Wang, Y.; Liu, Y.; He, J.; Zhang, Y. Redox-Neutral Photocatalytic Strategy for Selective C−C Bond Cleavage of Lignin and Lignin Models via PCET Process. *Sci. Bull.* **2019**, *64* (22), 1658−1666.
(56) Zhang, M.; Yang, L.; Yang, H.; An, G.; Li, G. Visible Light Mediated C(Sp3)-H Alkenylation of Cyclic Ethers Enabled by Aryl Ketone. *ChemCatChem* **2019**, *11* (6), 1606−1609.
(57) Hammes-Schiffer, S. Proton-Coupled Electron Transfer: Classification Scheme and Guide to Theoretical Methods. *Energy Environ. Sci.* **2012**, *5* (7), 7696−7703.
(58) Hammes-Schiffer, S. Theoretical Perspectives on Proton-Coupled Electron Transfer Reactions. *Acc. Chem. Res.* **2001**, *34* (4), 273−281.
(59) Mayer, J. M.; Hrovat, D. A.; Thomas, J. L.; Borden, W. T. Proton-Coupled Electron Transfer versus Hydrogen Atom Transfer in Benzyl/Toluene, Methoxyl/Methanol, and Phenoxyl/ Phenol Self-Exchange Reactions. *J. Am. Chem. Soc.* **2002**, *124*, 11142−11147.
(60) Skone, J. H.; Soudackov, A. V.; Hammes-Schiffer, S. Calculation of Vibronic Couplings for Phenoxyl/Phenol and Benzyl/Toluene Self-Exchange Reactions: Implications for Proton-Coupled Electron Transfer Mechanisms. *J. Am. Chem. Soc.* **2006**, *128* (51), 16655−16663.
(61) Sjödin, M.; Irebo, T.; Utas, J. E.; Lind, J.; Merényi, G.; Åkermark, B.; Hammarström, L. Kinetic Effects of Hydrogen Bonds on Proton-Coupled Electron Transfer from Phenols. *J. Am. Chem. Soc.* **2006**, *128* (40), 13076−13083.
(62) Litwinienko, G.; Ingold, K. U. Solvent Effects on the Rates and Mechanisms of Reaction of Phenols with Free Radicals. *Acc. Chem. Res.* **2007**, *40* (3), 222−230.
(63) Young, E. R.; Rosenthal, J.; Hodgkiss, J. M.; Nocera, D. G. Comparative PCET Study of a Donor-Acceptor Pair Linked by Ionized and Nonionized Asymmetric Hydrogen-Bonded Interfaces. *J. Am. Chem. Soc.* **2009**, *131* (22), 7678−7684.
(64) Damrauer, N. H.; Hodgkiss, J. M.; Rosenthal, J.; Nocera, D. G. Observation of Proton-Coupled Electron Transfer by Transient Absorption Spectroscopy in a Hydrogen-Bonded, Porphyrin Donor-Acceptor Assembly. *J. Phys. Chem. B* **2004**, *108*, 6315−6321.
(65) Morris, W. D.; Mayer, J. M. Separating Proton and Electron Transfer Effects in Three-Component Concerted Proton-Coupled Electron Transfer Reactions. *J. Am. Chem. Soc.* **2017**, *139* (30), 10312−10319.
(66) Hammes-Schiffer, S.; Iordanova, N. Theoretical Studies of Proton-Coupled Electron Transfer Reactions. *Biochim. Biophys. Acta, Bioenerg.* **2004**, *1655*, 29−36.
(67) Hammes-Schiffer, S.; Stuchebrukhov, A. A. Theory of Coupled Electron and Proton Transfer Reactions. *Chem. Rev.* **2010**, *110* (12), 6939−6960.
(68) Di Meo, F. Di; Lemaur, V.; Lazzaroni, R.; Duroux, J.; Olivier, Y.; Trouillas, P. Free Radical Scavenging by Natural Polyphenols: Atom versus Electron Transfer. *J. Phys. Chem. A* **2013**, *117*, 2082−2092.
(69) Hanthorn, J. J.; Valgimigli, L.; Pratt, D. A. Incorporation of Ring Nitrogens into Diphenylamine Antioxidants: Striking a Balance between Reactivity and Stability. *J. Am. Chem. Soc.* **2012**, *134* (20), 8306−8309.
(70) DiLabio, G. A.; Johnson, E. R. Lone Pair-π and π-π Interactions Play an Important Role in Proton-Coupled Electron Transfer Reactions. *J. Am. Chem. Soc.* **2007**, *129* (19), 6199−6203.
(71) Yuasa, J.; Yamada, S.; Fukuzumi, S. One-Step versus Stepwise Mechanism in Protonated Amino Acid-Promoted Electron-Transfer Reduction of a Quinone by Electron Donors and Two-Electron Reduction by a Dihydronicotinamide Adenine Dinucleotide Analogue. Interplay between Electron Transfer and Hydrogen Bonding. *J. Am. Chem. Soc.* **2008**, *130* (17), 5808−5820.
(72) Alligrant, T. M.; Alvarez, J. C. The Role of Intermolecular Hydrogen Bonding and Proton Transfer in Proton-Coupled Electron Transfer. *J. Phys. Chem. C* **2011**, *115* (21), 10797−10805.
(73) Nomrowski, J.; Wenger, O. S. Photoinduced PCET in Ruthenium-Phenol Systems: Thermodynamic Equivalence of Uni- and Bidirectional Reactions. *Inorg. Chem.* **2015**, *54* (7), 3680−3687.
(74) Nguyen, T. M.; Nicewicz, D. A. Anti-Markovnikov Hydroamination of Alkenes Catalyzed by an Organic Photoredox System. *J. Am. Chem. Soc.* **2013**, *135* (26), 9588−9591.
(75) Margrey, K. A.; Nicewicz, D. A. A General Approach to Catalytic Alkene Anti-Markovnikov Hydrofunctionalization Reactions via Acridinium Photoredox Catalysis. *Acc. Chem. Res.* **2016**, *49* (9), 1997−2006.
(76) Nguyen, T. M.; Manohar, N.; Nicewicz, D. A. Anti-Markovnikov Hydroamination of Alkenes Catalyzed by a Two-Component Organic Photoredox System: Direct Access to Phenethylamine Derivatives. *Angew. Chem., Int. Ed.* **2014**, *53* (24), 6198−6201.
(77) Gagliardi, C. J.; Murphy, C. F.; Binstead, R. A.; Thorp, H. H.; Meyer, T. J. Concerted Electron Proton Transfer (EPT) in the Oxidation of Cysteine. *J. Phys. Chem. C* **2015**, *119* (13), 7028−7038.
(78) Kuss-Petermann, M.; Wenger, O. S. Mechanistic Diversity in Proton-Coupled Electron Transfer between Thiophenols and Photoexcited [Ru(2,2′-Bipyrazine)3]2+. *J. Phys. Chem. Lett.* **2013**, *4* (15), 2535−2539.
(79) Gesmundo, N. J.; Grandjean, J. M. M.; Nicewicz, D. A. Amide and Amine Nucleophiles in Polar Radical Crossover Cycloadditions: Synthesis of γ-Lactams and Pyrrolidines. *Org. Lett.* **2015**, *17* (5), 1316−1319.
(80) Qiu, G.; Knowles, R. R. Understanding Chemoselectivity in Proton-Coupled Electron Transfer: A Kinetic Study of Amide and Thiol Activation. *J. Am. Chem. Soc.* **2019**, *141*, 16574−16578.
(81) Ruccolo, S.; Qin, Y.; Schnedermann, C.; Nocera, D. G. General Strategy for Improving the Quantum Efficiency of Photoredox Hydroamidation Catalysis. *J. Am. Chem. Soc.* **2018**, *140* (44), 14926−14937.
(82) Gschwind, R. M.; Armbrüster, M.; Zubrzycki, I. Z. NMR Detection of Intermolecular NH···OP Hydrogen Bonds between

https://dx.doi.org/10.1021/jacs.0c08673
J. Am. Chem. Soc. 2021, 143, 724−735

Guanidinium Protons and Bisposphonate Moieties in an Artificial Arginine Receptor. *J. Am. Chem. Soc.* **2004**, *126* (33), 10228−10229.
(83) Sharif, S.; Denisov, G. S.; Toney, M. D.; Limbach, H.-H. NMR Studies of Coupled Low-and High-Barrier Hydrogen Bonds in Pyridoxal-5′-Phosphate-Enzyme Model Systems in Polar Solution. *J. Am. Chem. Soc.* **2007**, *129* (11), 6313−6327.
(84) Steiner, T. The Hydrogen Bond in the Solid State. *Angew. Chem., Int. Ed.* **2002**, *41* (1), 48−76.
(85) Prins, L. J.; Reinhoudt, D. N.; Timmerman, P. Noncovalent synthesis using hydrogen bonding. *Angew. Chem. Int. Ed.* **2001**, *40* (13), 2382−2426.
(86) Harris, T. K.; Zhao, Q.; Mildvan, A. S. NMR Studies of Strong Hydrogen Bonds in Enzymes and in a Model Compound. *J. Mol. Struct.* **2000**, *552* (1), 97−109.
(87) Greindl, J.; Hioe, J.; Sorgenfrei, N.; Morana, F.; Gschwind, R. M. Brønsted Acid Catalysis - Structural Preferences and Mobility in Imine/Phosphoric Acid Complexes. *J. Am. Chem. Soc.* **2016**, *138*, 15965−15971.
(88) Sorgenfrei, N.; Hioe, J.; Greindl, J.; Rothermel, K.; Morana, F.; Lokesh, N.; Gschwind, R. M. NMR Spectroscopic Characterization of Charge Assisted Strong Hydrogen Bonds in Brønsted Acid Catalysis. *J. Am. Chem. Soc.* **2016**, *138* (50), 16345−16354.
(89) Chen, K.; Berg, N.; Gschwind, R.; König, B. Selective Single C(Sp3)-F Bond Cleavage in Trifluoromethylarenes: Merging Visible-Light Catalysis with Lewis Acid Activation. *J. Am. Chem. Soc.* **2017**, *139*, 18444−18447.
(90) Hunter, C. A. Quantifying Intermolecular Interactions: Guidelines for the Molecular Recognition Toolbox. *Angew. Chem., Int. Ed.* **2004**, *43* (40), 5310−5324.
(91) The broad ^{15}N−H signal was processed using a Gaussian window function for better resolution (Figure 2b).
(92) Bordwell, F. G.; McCallum, R. J.; Olmstead, W. N. Acidities and Hydrogen Bonding of Phenols in Dimethyl Sulfoxide. *J. Org. Chem.* **1984**, *49* (49), 1424−1427.
(93) Bondi, A. Van Der Waals Volumes and Radii. *J. Phys. Chem.* **1964**, *68* (3), 441−451.
(94) Notably, the ammonium is partially separated from dimer **1** in the thiophenol/base mixture (for comparison of the DOSY values, see SI).
(95) Dadová, J.; Kümmel, S.; Feldmeier, C.; Cibulková, J.; Pažout, R.; Maixner, J.; Gschwind, R. M.; König, B.; Cibulka, R. Aggregation Effects in Visible-Light Flavin Photocatalysts: Synthesis, Structure, and Catalytic Activity of 10-Arylflavins. *Chem. - Eur. J.* **2013**, *19* (3), 1066−1075.
(96) The comparison of MD derived diffusion coefficients of the different species yielded additional information about the thiophenolate. As the values for the thiolate are significantly smaller than those of PhSH, the complexation of the thiolate was verified.
(97) Please be aware that Ph_2S_2 and acid can produce PhSH upon irradiation with blue light. That means that, in photocatalysis acid, Ph_2S_2 and PhSH can interconvert into each other. Nevertheless, separation into acid and Ph_2S_2 allows for a selective tuning of the proton density and the H-bond networks in the ground state.
(98) Bartling, H.; Eisenhofer, A.; König, B.; Gschwind, R. M. The Photocatalyzed Aza-Henry Reaction of N-Aryltetrahydroisoquinolines: Comprehensive Mechanism, H●- versus H+-Abstraction, and Background Reactions. *J. Am. Chem. Soc.* **2016**, *138* (36), 11860−11871.

https://dx.doi.org/10.1021/jacs.0c08673
J. Am. Chem. Soc. 2021, 143, 724−735